THE PRACTICAL APPLICATION OF CFD IN THE DESIGN OF INDUSTRIAL CENTRIFUGAL IMPELLERS

by

James M. Sorokes

Supervisor, Aerodynamics

Dresser-Rand

Olean, New York

James M. Sorokes received a B.S. degree from St. Bonaventure University (1976). Since graduation, he has been employed at Dresser-Rand (formerly Dresser-Clark) for 17 years in the Aerodynamics Group. He has been Supervisor of Aerodynamics since 1984. His primary job functions include the development, design, and analysis of all rotating and stationary aerodynamic components of centrifugal compressors.

Mr. Sorokes is a member of AIAA, ASM, ASME, and the ASME Turbomachinery Committee. He has written or has been a coauthor on nine technical papers including four for ASME. He also holds two U.S. patents.

ABSTRACT

The practical application of computational fluid dynamics software in the industrial turbomachinery design process is discussed. Such codes have been used for years in the design of gas turbines, but have long been underutilized by the process compressor world. New streamlined or specialized solvers have been developed which minimize the effort required to obtain CFD results on axisymmetric components, i.e., impellers, diffusers, etc. One such code (BTOB3D developed by Dr. William Dawes) and the post-processors and plots used to interpret the results are described. Three sample cases are offered to illustrate the use of the code for comparison of designs; and for flow visualization. Finally, comments are offered regarding the present limitations of CFD tools.

INTRODUCTION

Compressor aerodynamic designers are continually striving to gain a better understanding of the behavior of flow as it passes through the various turbomachinery components. For years, the workhorse of the aero designer was the streamline curvature code. These codes typically calculate the flowfield in two dimensions (most often hub-to-shroud) and then estimate the third dimension (blade-to-blade). Such analyses yield a good overview of the velocity and pressure profiles through a component. However, given the three-dimensional nature of flow, two-dimensional codes, despite good approximations for the third dimension, will miss the finer details of the flowfield.

The development of three-dimensional computational fluid dynamics (CFD) codes has provided aerodynamic engineers with a powerful turbomachinery design and analysis tool. Algorithms have been developed that permit any flowfield to be calculated in all three dimensions. There are now commercially available packages that allow virtually any flow passage to be analyzed; giving the analyst tremendous insight into the flowfield characteristics of a component. Still, this new capability does not come without a price. To perform an analysis, the passage must be modelled or meshed using a grid similar to those developed for finite element stress analyses. However, in stress analysis, the solid is modelled while in computational fluid dynamics, the gas path must be meshed. Many of the generalized codes require extensive models (i.e., large or dense grids) and, as a consequence, necessitate large computers and disk capacity. Therefore, some analyses can require months of effort. Should the design cycle allow for such durations, the generalized solvers are an acceptable option. However, most industrial centrifugal compressors are frequently multistage configurations that require varying numbers of impeller designs. Some units can require as many as 12 wheels of varying flowrates. In addition, some processes require more than one multistage compressor. Further, if one considers the number of turbomachines sold by the process compressor manufacturer, one can begin to appreciate the large number of different impeller analyses that may be undertaken. Given this vast number, it is obviously impractical to spend months or even weeks analyzing each individual impeller design.

However, several specialized tools have been developed to ease the modelling and computational effort. With these codes, it is possible to generate an input case and complete the computer runs in one or two days. This reduced cycle time makes it possible and practical to use CFD as an everyday design tool.

The use is discussed of one such specialized solver; the Dawes code, BTOB3D; in the design and analysis of industrial centrifugal impellers. A brief description of the CFD code is offered together with an overview of the input. Remarks are included about how the input is streamlined specifically for axisymmetric components. The author also comments on the need for adequate postprocessors and describes the types of plots used by analysts to review CFD results.

The author continues with a discussion of the results of recent analyses that illustrate the practical application of the code. A further example is offered to illustrate the use of the CFD code as a visualization tool. Finally, before concluding remarks, comments are offered concerning keeping the proper perspective on CFD results.

THE DAWES CODE, BTOB3D

The code was developed by Dr. William Dawes of Whittle Laboratory at Cambridge University in England. The solution is based on the time-dependent Reynolds-averaged Navier-Stokes equations. The Dawes code employs the Baldwin-Lomax turbulence model. Note, it is not the intent here to derive nor even describe the governing equations or algorithms used in the Dawes code. Instead, the author concentrates on the application of BTOB3D. For those interested, several papers are listed in the REFERENCES section that provide detailed descriptions of the equations involved.

BTOB3D provides a fully 3-D solution, and can be used to analyze the flow field through any axisymmetric bladed passage.

BTOB3D cannot be used to analyze nonaxisymmetric components such as inlet ducts, discharge volutes, or the like. Therefore, the code can be applied to rotor blades and stator vanes in axial compressors and turbines. Further, centrifugal compressor impeller, vaned diffuser, and return channel passages can be calculated. Impellers may be shrouded or unshrouded; however, if splitter blades are required, a separate version of the code, BTOB3DSP, must be used. Note, all applications described herein are shrouded impellers having no splitter blades.

Program Input

Input for the code is broken down into three major sections. The first section contains indicators that control program operation. Component geometry is specified in the second section while boundary conditions make up the third portion.

Indicators specify the size of the input grid, number of time steps (iterations) to be performed, geometric input options, output options, etc.

The code takes advantage of the symmetry of the bladed passage to ease both the geometric input and calculation process. For example, when modelling an impeller or diffuser, only one passage need be modelled. The code then assumes that all other passages are equivalent; i.e., geometry and boundary conditions. Geometric input is further simplified should the impeller blading be defined by straight line elements (Figure 1). Here, only r, z, and r for the endpoints of the line elements need be input. BTOB3D then interpolates along the line elements for the remainder of the blading definition.

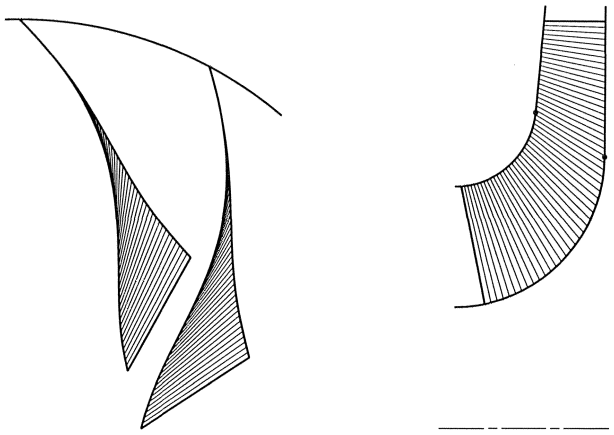

Figure 1. Impeller Blading Defined by Straight Line Elements.

Upstream and downstream geometries also must be included to set up the appropriate conditions into the component of interest. Again using an impeller analysis as an example, the user must include the upstream configuration (axial or radial inlet guide contour) and some definition of the exit geometry (specified as a vaneless section).

Boundary conditions are specified as inlet pressures, temperatures, and velocity vectors (axial, radial, tangential). The exit boundary condition is specified as the static pressure at the exit of the modelled geometry. In addition, gas characteristics, Reynolds number, operating speed, and other factors related to the turbulence model must be entered.

Program Output

BTOB3D output consists of three basic files. The first is a printer file which provides select results of the iterations. A user will typically scan this file to ensure that the solution converged properly or if iteration problems were encountered. The second file is an iteration history file that may also be used to check convergence. The third, and most important file, contains the plot dump. This file is used by the post-processors (plotting system) and also may be used as a re-start input file should additional iterations be necessary to achieve convergence.

An adequate 3-D plotting system is essential for interpreting CFD results. Without such, the output files are meaningless columns of numbers. A user would be hard pressed to understand the 3-D flowfield by reviewing literally hundreds of pages of printed output. Several excellent plotting systems (too numerous to list herein) for post-processing BTOB3D results are available commercially. For those interested, the plots contained in this paper were generated by PLOT3D and POSTDAWES.

The plot file contains the grid coordinates and all parameters necessary to analyze the flowfield—i.e., velocities, pressures, temperatures, entropies, etc. The choice of plots used to study the flowfield depends entirely on the preferences of the analyst. The following sections describe some of the typical plots employed to review CFD results. Included are comments regarding how each plot is used to judge the flowfield.

• Velocity vector plots are one of the most popular plots for CFD users. Velocities are represented as arrows (or vectors) which show the direction of the flow. The length of the arrow reflects the magnitude of the velocity. The analyst will review the vectors along impeller blade suction and pressure surfaces (I planes) and along hub and shroud contours (K planes). These planes are illustrated in Figures 2 (a) and (c). Vector plots at various planes perpendicular to the streamwise direction (J planes) are often generated (Figure 2 (b)). The analyst will note any regions of low or reverse velocities which indicate stalled or recirculating flow.

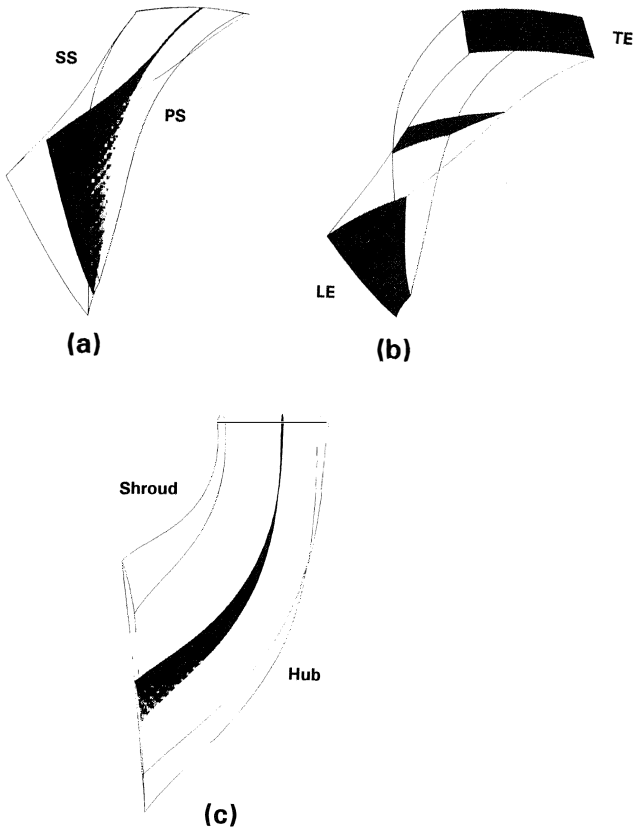

Figure 2. Definition of Plotting Planes. (a) I plane; (b) J plane; (c) K plane. See NOMENCLATURE.

• Mach Number contour plots are another standard format. The plots take on the appearance of a topographical map. Contour plots typically come in one of two forms: a) color contours or b) labeled line contours with either type including a colored or numbered key to distinguish the mach number level. Again, plots are normally generated along various I, J, and K planes. The reviewer will look for any regions of high mach number or possible shocks. However, of equal interest are low mach number zones which could indicate separated zones, stall cells, or wake regions.

• Pressure and/or temperature contour plots can be beneficial to aerodynamicists along with stress and heat transfer concerns. Obviously, the stress analyst will be interested in the forces acting upon the vane surfaces. Similarly, the heat transfer specialist can use the temperature results to assess the thermal effects on the component. Again, plots are typically generated along various I, J, and K planes.

• Entropy plots are growing in acceptance since entropy is a convenient way of portraying the state of disorder of the flowfield; the higher the entropy, the more disturbed the flow profile. For example, the region around a shock wave will show a high entropy level. Similarly, wake regions will also appear as increased entropy zones. In short, by searching for regions of higher entropy, the analyst can quickly identify problems in the flow profile regardless of their source. Again, I, J, and K planes are typically plotted.

• Streakline plots (pseudo-particle traces) are a very convenient way of visualizing how the flow travels through a component. These plots are almost always done along I or K planes with particles released at a specified J plane. Lines or streaks trace the path that a particle would follow, had it been released in the flow stream at the specified location. Typically, arrays of "particles" are released across the blade leading edge on pressure and suction surfaces or along the hub or shroud surfaces between two adjacent blades. Again, such plots ease the identification of flow reversal, separation cells, vortices, etc.

Examples of several of these plots will be seen in the cases described in the remainder of the paper. As noted, these plots are typically in color. However, given the printing limitations imposed, all plots herein are in black and white. This does detract somewhat from one's ability to interpret the results. However, the general trends are still visible.

COMPUTER HARDWARE

For those interested in such matters, the CFD runs required for this paper and all postprocessing were done on a Silicon Graphics Model 340 Workstation. The system is configured with four processors (though BTOB3D only uses one at a time), 64 megabytes of RAM, and over 2.4 gigabytes of disk space. Execution times varied from seven to 24 hr, depending primarily on grid density. The typical input preparation time was two to three days; however, with new preprocessors, this time has been reduced to two to three hours. Such elapsed times make the application of CFD a practical alternative for the industrial designer.

COMPARISON OF IMPELLER DESIGNS

This first example demonstrates how the CFD code was used during an impeller redesign effort. The original wheel exhibited a droop in the pressure rise characteristic as flow was reduced from design point. Therefore, a new impeller was developed and the droop was eliminated. Details of the performance characteristics were presented by Sorokes and Welch and, therefore, will not be discussed in detail here. However, for those unfamiliar with the prior work, the following brief description of the two impellers is offered.

The impellers are of moderate flow coefficient ($\phi = 0.093$). The original impeller is shown in Figure 3. The blading was defined using a torus section and the blade was inclined relative to the hub plane to achieve the desired inlet angles. The reader should note the high level of curvature (tight radius) along the shroud surface.

The new design is shown in Figure 4. The reader will immediately note the reduction in shroud curvature (larger radius). In addition, the new blading is an arbitrary shape; that is, the blade is generated using lines in space and cannot be defined using any geometric figure.

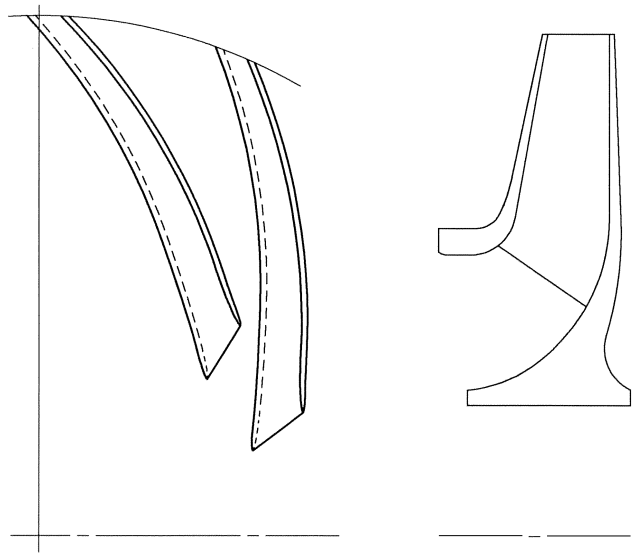

Figure 3. The Original Impeller.

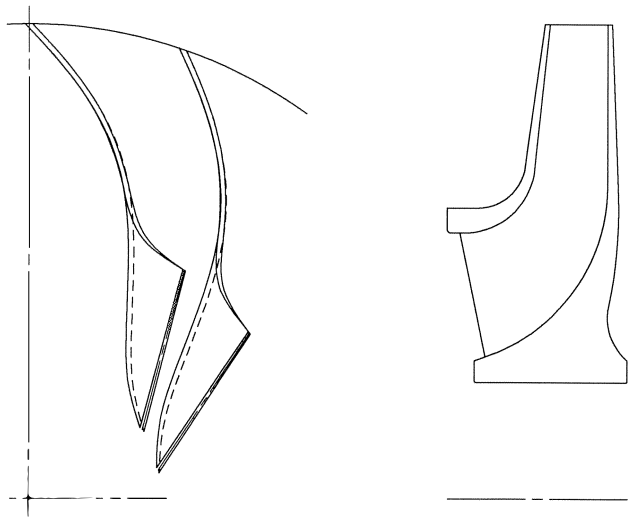

Figure 4. The New Impeller.

To properly compare the original design to the replacement, CFD analyses were conducted at three operating conditions: design flow; 80 percent; and 120 percent of design flow. However, to conserve space, only the design flow results for the initial and final impellers will be discussed in detail. Operating speed and inlet conditions (pressure, temperature) were also held constant for all runs.

CFD analyses of the initial design were completed first. The grid generated for the initial impeller as shown in Figure 5 (a) and (b). For ease of viewing the grid shown in Figure 5 (a) shows the grid points that lie on the surface of the impeller blades. The grid spacing in the blade to blade direction is given in Figure 5 (b); note that hub and shroud are labeled for clarity. The computational grid is assembled by projecting the grid points shown in both the hub-to-shroud and blade-to-blade direction; in essence creating a solid passage of grid points.

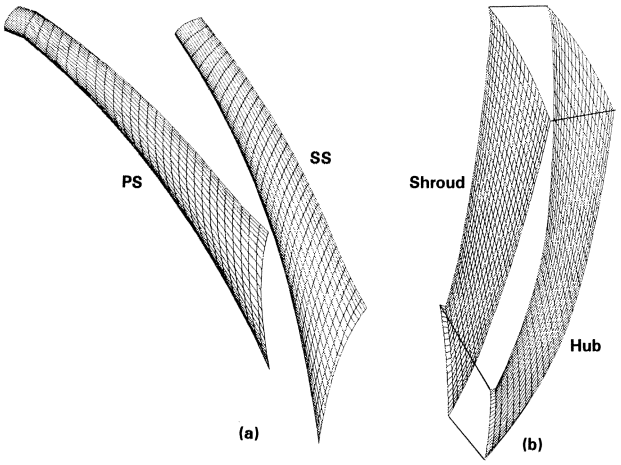

Figure 5. Grid For Original Impeller Analysis. (a) grid spacing along blade surfaces; (b) grid spacing along hub and shroud surfaces.

Results pointed out several deficiencies in the flowfield including high mach number areas (i.e., mach number greater than 0.7), separation or reverse flow regions, and an extremely large exit wake. For example, the mach number distribution along the suction surface of the blade is shown in Figure 6. Note the high mach number region near the shroud leading edge and subsequent large zone of near zero mach number. While transonic or supersonic designs are common in gas turbine applications, they are not desirable in the process industry, due to their limited flow range. Therefore, process compressor designers typically avoid mach number levels much greater than 0.7 to 0.8. Further, the velocity vector plots in Figure 7 clearly show flow reversal along the suction surface as many of the vectors point back toward the impeller inlet. Again, such separation cells will cause excess losses in the impeller. Further, as the flowrate is reduced further, these separation zones grow increasingly larger until full separation or stall occurs.

However, the most disturbing result of the analysis was the large wake (region of depressed mach number or increased entropy) that appears to occupy nearly 50 percent of the impeller exit area. This wake region can be seen in both Figures 8 and 9. In Figure 8, the large wake is seen as the depression in the 3-D contour map of exit mach number. The formation of (and increase in) the wake can be seen in Figure 9, which shows entropy contours at various streamwise planes (J-direction); the wake region begins to form very near the impeller inlet and grows to the large region apparent at the exit.

The secondary flows present in all centrifugal impellers will always cause the formation of a wake region in each blade passage. This wake region will grow in size with reduced flowrate and will contribute to reduced pressure rise and ultimately, impeller stall. However, in a well-designed wheel, the wake region occupies a much smaller portion of the impeller exit area; typically 10 percent to 20 percent. Given the extremely large size of the wake exhibited by the original design even at design flow, one can easily understand the discontinuity in pressure rise. Clearly, the initial design manifested several detrimental characteristics that would lead to the observed performance deficiency.

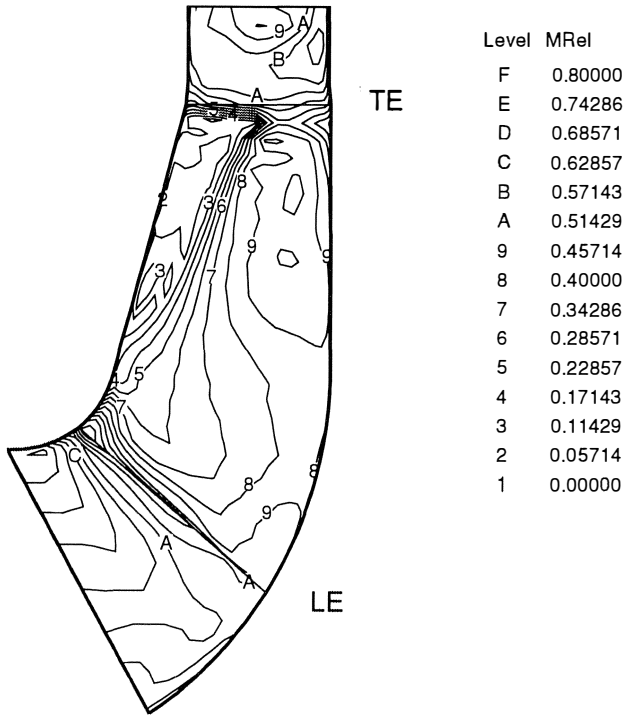

Figure 6. Suction Surface Mach Number Distribution (Original Design).

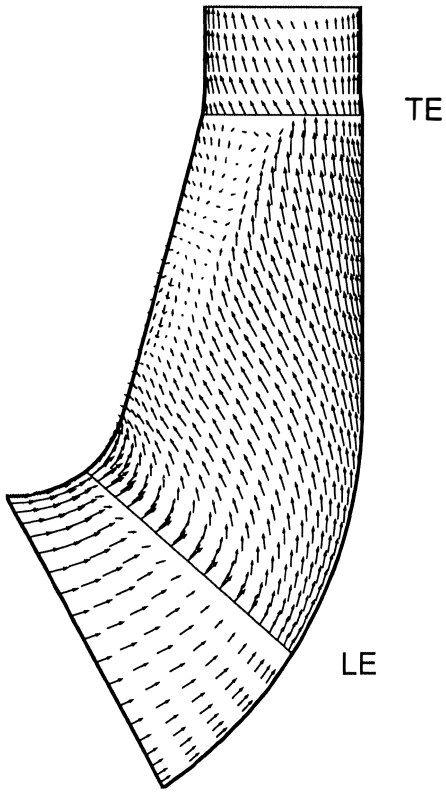

Figure 7. Suction Surface Velocity Vector Plot (Original Design).

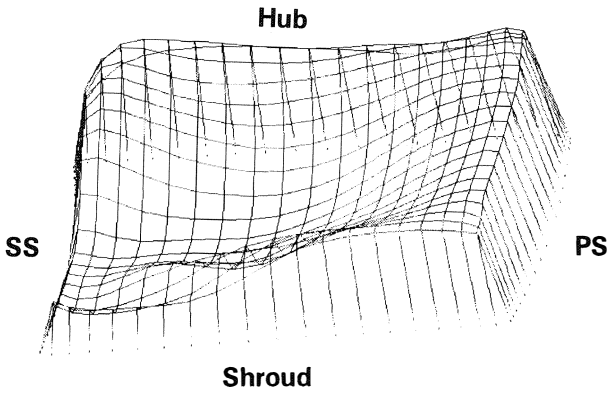

Figure 8. Impeller Exit Mach Number Contour (Original Design).

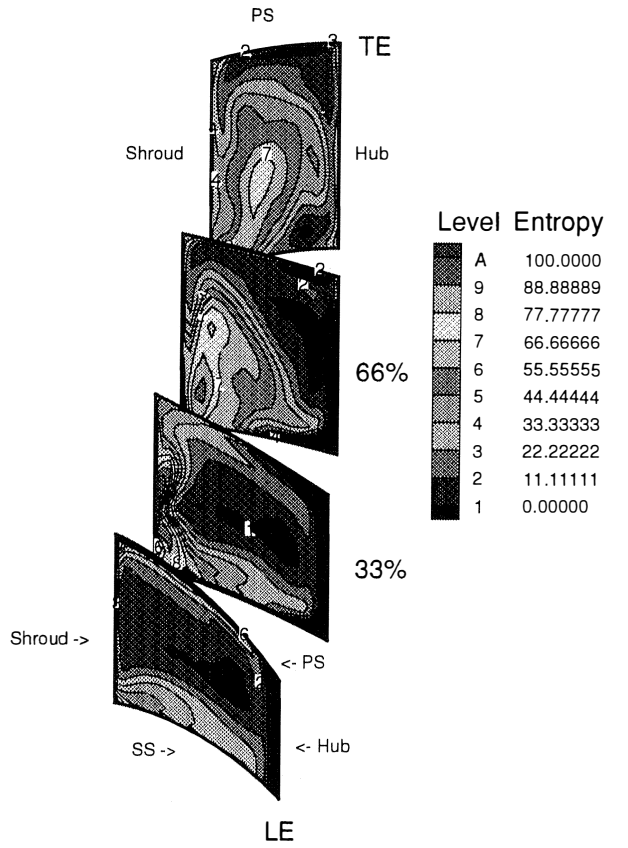

Figure 9. Entropy Levels at Various J Planes (Original Design).

Several alternate geometries were developed and analyzed with the objectives being to: a) reduce the peak mach number; b) eliminate or reduce the amount of recirculation; and c) reduce the size of the exit wake region. CFD results for the configuration yielding the most improvement are presented in the following discussion.

The plots presented for the new design follow the same format as those of the initial impeller. Recall, the CFD analyses for both impellers (initial and alternate) were run under the same boundary or operating conditions. Therefore, by comparing the results of the two studies, the reader can see the advantages of the new design.

The grid used for the alternate design is presented in Figure 10 (a) and (b); again, section (a) shows the grid distribution along the blades while (b) shows the hub and shroud gridding. The mach

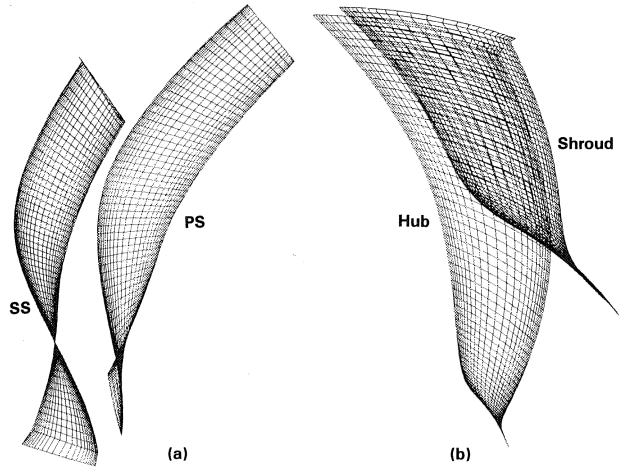

Figure 10. Grid For Redesigned Impeller Analysis. (a) grid spacing along blade surfaces; (b) grid spacing along hub and shroud surfaces.

number distribution is shown in Figure 6 along the suction surface. Note that the maximum mach number has been reduced dramatically and that the region of low mach number is also reduced; i.e., the wake region is smaller. The velocity vector plot (Figure 12) still shows a very small region of reverse flow, but not of the size seen in the earlier design. Further, the 3-D contour plot of impeller exit mach number. A much smaller depression or wake region is shown in Figure 13; the wake now occupies approximately 20 percent of the exit area.

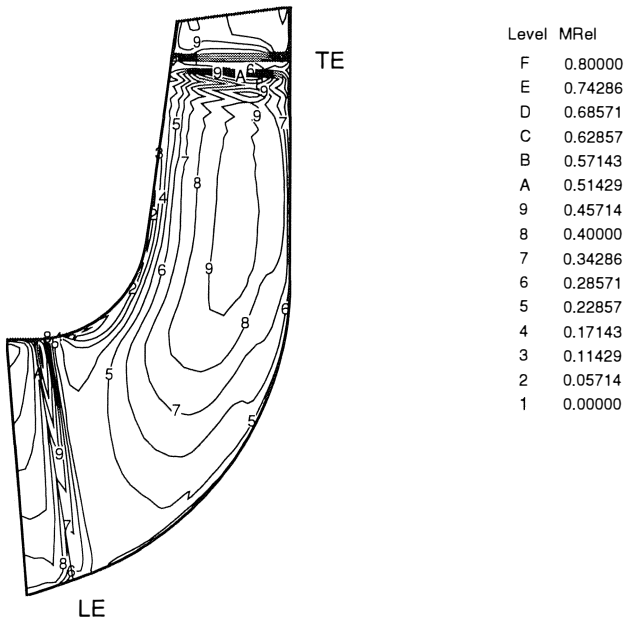

Figure 11. Suction Surface Mach Number Distribution (New Design).

Finally, the entropy plot (Figure 14), shows the growth of the wake region. While still very apparent, the entropy levels are significantly reduced; again indicating a more well behaved exit flow. In the final analysis, the objectives of the redesign had been achieved as the CFD results have shown the alternate design to be an improvement over the original impeller.

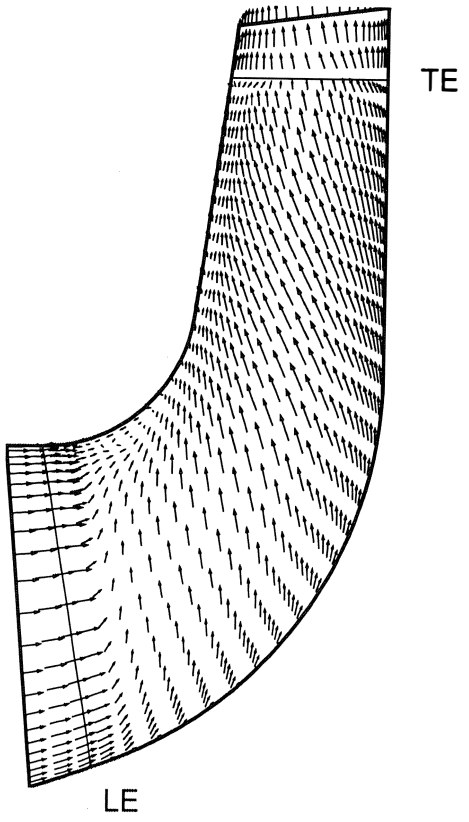

Figure 12. Suction Surface Velocity Vector Plot (New Design).

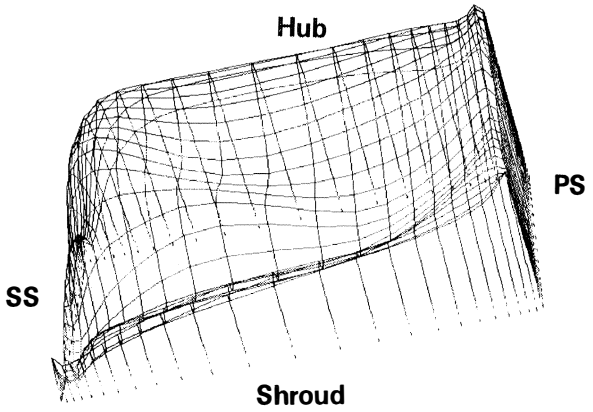

Figure 13. Impeller Exit Mach Number Contour (New Design).

As noted previously, other comparative runs were done at higher and lower flowrates as well as higher and lower operating speeds. Comparative results at these conditions will not be presented. However, two important results were obtained. First, under high flow conditions, the new designs yielded lower mach numbers than the original impeller. Therefore, the new design should have more capacity range to choke than the earlier impeller. Second, at the reduced flow condition, the wake region and level of recirculating flow were much smaller for the new design than on the original wheel. Consequently, one would expect the new impeller to exhibit better range to surge or stall. In short, the new design offered better flow range and higher performance over that improved range.

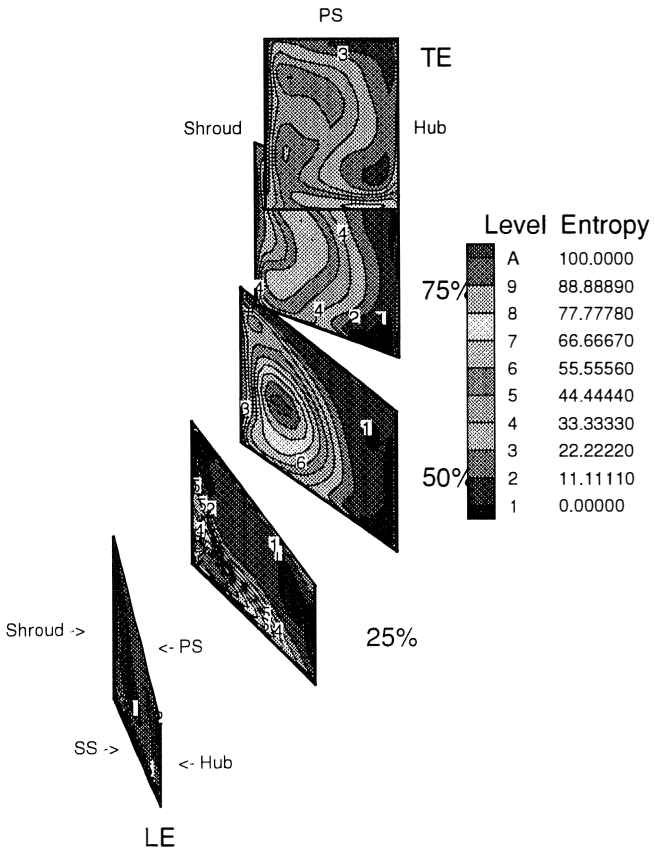

Figure 14. Entropy Levels At Various J Planes (New Design).

As a final note, the alternate design described herein is the impeller whose test results were presented by Sorokes and Welch. In short, the improvement seen in CFD results was confirmed by the test results as shown in Figure 15. That is, the droop in the pressure rise characteristic was eliminated. Given these results, it is obvious that a CFD code can be extremely valuable in assessing the soundness of new designs. That is, given a firm set of assessment criteria (more on this later), unacceptable designs can be rejected without expending considerable time and dollars to physically test various alternatives.

A Low Flow CFD Result

Before moving on to the next example, the following section compares the CFD low flow (nearer surge) and design flow results

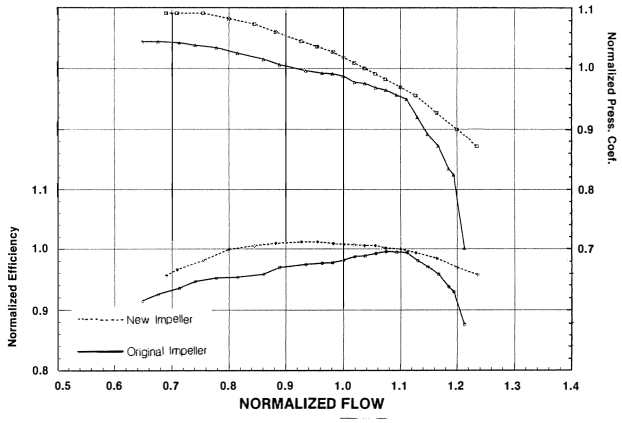

Figure 15. Performance Test Results (Original vs *New Impeller).*

for the new impeller. The comparison is made to portray the degradation of the flowfield as the impeller approached stall or surge flow. As noted, the new design yielded good performance on test and exhibited none of the adverse characteristics of the earlier impeller. This is an important point considering the CFD results obtained at the reduced flow.

As noted previously, reduced flowrates will cause larger wake regions and will promote the conditions necessary for separated or stalled zones in the impeller passage. These phenomena cause a reduction in impeller performance and contribute to the reduction in rise to surge when the impeller is operated below its design flowrate. To illustrate this situation, consider the mach number, entropy, and velocity vector plots shown in Figures 16, 17, and 18.

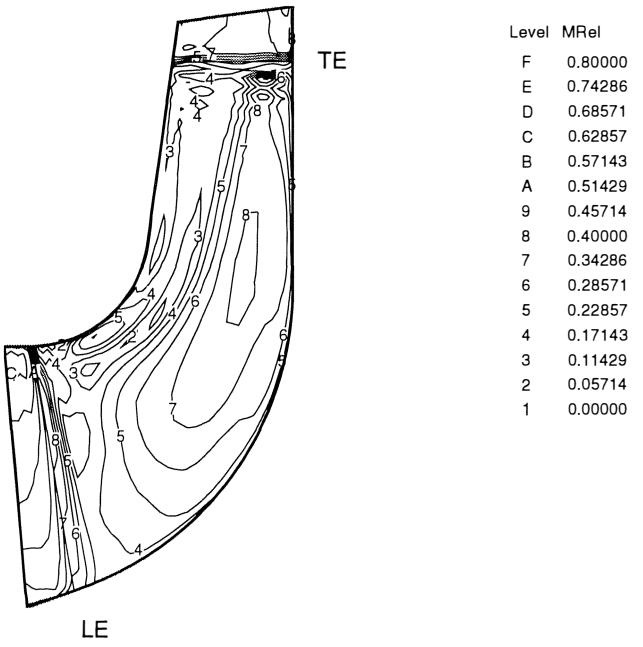

Figure 16. Suction Surface Mach Number Distribution (New Design—Low Flow).

Most notable in Figure 16 is the very large low mach number region along the shroud suction surface. This suggests a large separation from the shroud surface at this operating condition. Actually, the higher mach number islands along the shroud (contour levels 4 and 5) represent high velocity flow in the reverse direction! Compare this distribution to the design flow case shown in Figure 11. Likewise, the entropy results (Figure 17) depict the formation of a large wake region at low flow. Again, compare these results to those obtained at design flow (Figure 14). The wake is much smaller for the design case.

Finally, the velocity vector plots (Figure 18) clearly show a large region of reverse flow along the suction surface. In addition, there is an obvious "vortex" in the vectors just downstream of the leading edge. At design conditions (Figure 12), there was little or no reverse flow; indicating a much better behaved flowfield.

As stated, the characteristic observed at the low flow case are precursors to impeller stall and will occur in any impeller as the flowrate is reduced from design. Therefore, despite the improved performance of the new design, the impeller will exhibit the wake regions and separated zones at near surge conditions. By performing CFD analyses at these low flow cases, the analyst can better understand off-design impeller performance.

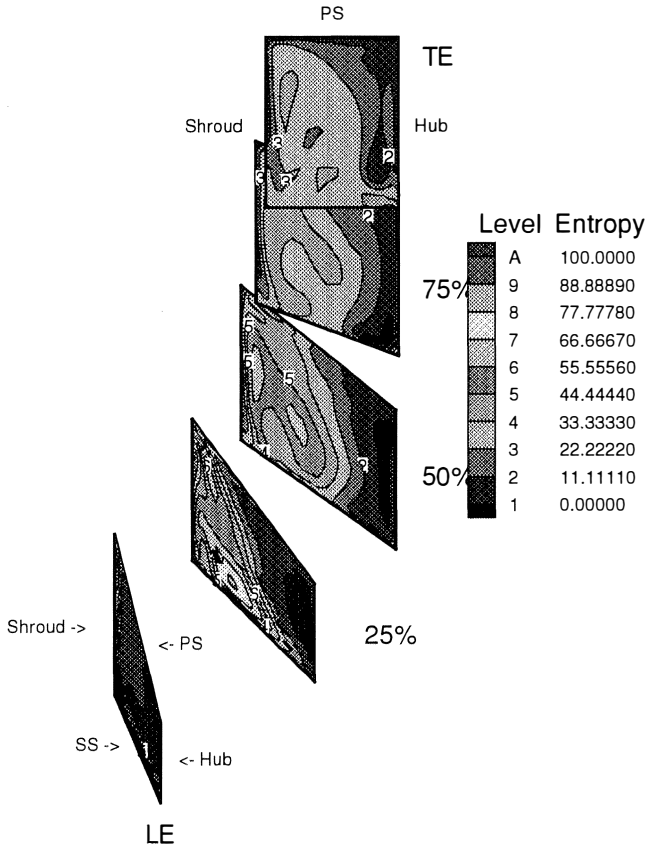

Figure 17. Entropy Levels At Various J Planes (New Design—Low Flow).

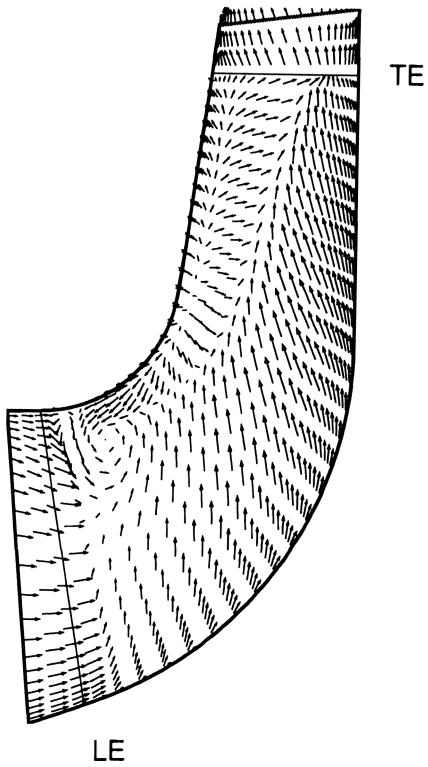

Figure 18. Suction Surface Velocity Vector Plot (New Design—Low Flow).

JUDGING MANUFACTURING DEVIATIONS

The second example will further illustrate the use of the CFD code as a comparative tool. In this case, analyses were performed to judge the effect of a manufacturing deviation on impeller performance. The impellers in question are small capacity wheels which employ simple circular arc style blading. The impeller is shown in Figure 19. During construction, the blades in some production wheels were found to be inclined relative to their designed position. While the desired blade has an angle of 90 degrees relative to the hub, the actual blades were at an angle of 100.5 degrees. Concerns were expressed that this deviation might cause detrimental effects on the impeller performance. For instance, flow might migrate across the blades due to the lean; causing separation from the hub surface.

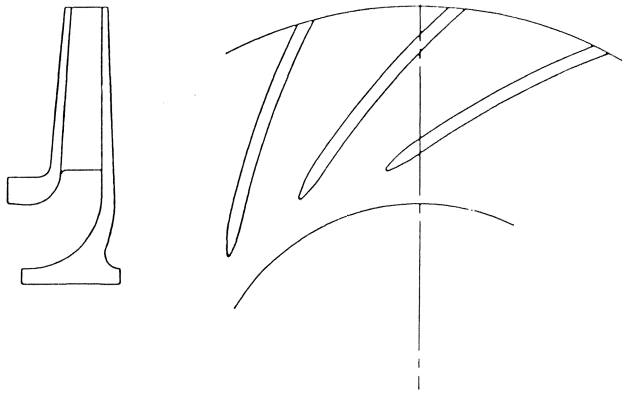

Figure 19. Low Flow Coefficient Impeller with Circular Arc Blading.

To determine the effect of the deviation, impeller models were generated with and without the blade lean. The computational grids are shown in Figures 20 and 21 for the correct *vs* erroneous impeller, respectively. The deviation becomes more visible when viewing the grid directly into the impeller exit. Again, note that the blade in Figure 21 is not perpendicular to the hub plane.

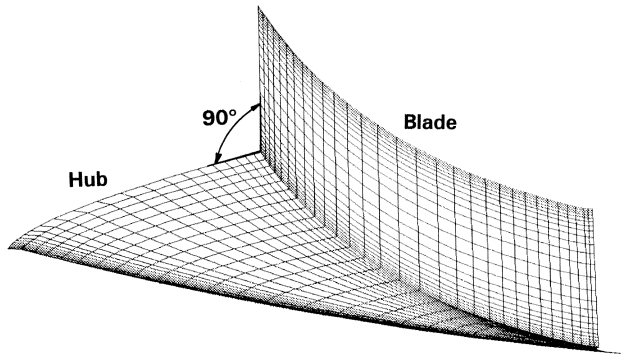

Figure 20. Analysis Grid for Impeller with Correct Blading.

Analyses were run for both configurations at equivalent boundary or inlet conditions. For reference, the subject impellers were to be operating at a very low tip mach number ($U_2/A_o = 0.5$). Also, as in the impeller design comparison above, plots of mach number and velocity vectors are used to compare the resulting flowfields.

It quickly became evident that the lean had little or no effect on the flow profile at the required operating speed. To illustrate, the reader is asked to review the mach number and velocity vector plots shown in Figures 22, 23, 24, and 25. In all cases, the (a) portion of the figure shows the results for the correct blade while the (b) portion depicts the flowfield for the tilted blades. Clearly, there are no significant differences in the visible patterns. Therefore, though not conforming to design specification, the impeller blade lean was judged to be of no cause for concern in the required application.

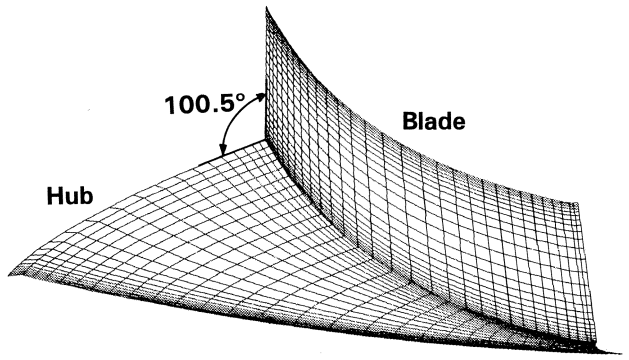

Figure 21. Analysis Grid for Impeller with Blade Lean (Deviation).

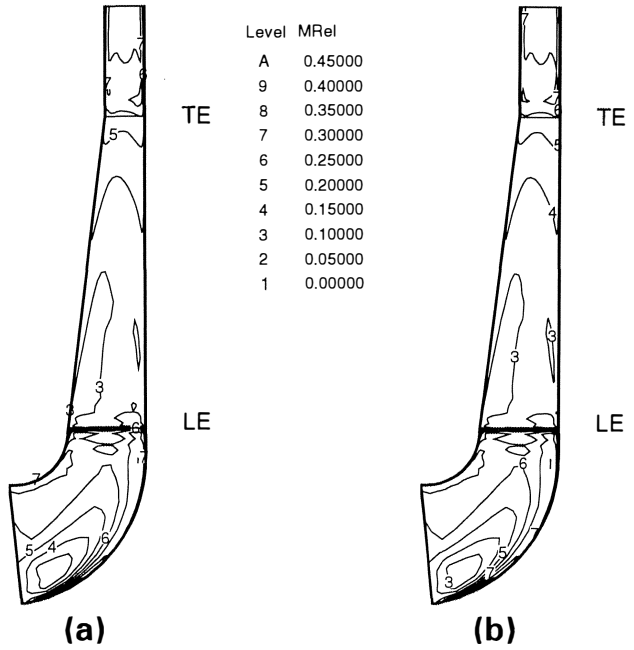

Figure 22. Pressure Surface Mach Number Contours. (a) correct blading; (b) blade with lean.

Subsequent to the CFD study, the impellers were installed in a production unit. Though no detailed component data was taken, the performance on the stages that contained the subject impellers matched our earlier experience with impellers having correct blading. In short, the test results confirmed the CFD-based conclusion that the blade lean would have no adverse effects on performance. Again, the acceptability of components was determined without costly test programs.

Before moving on to the final sample case, both preceding examples illustrate the use of the CFD code as a comparative tool.

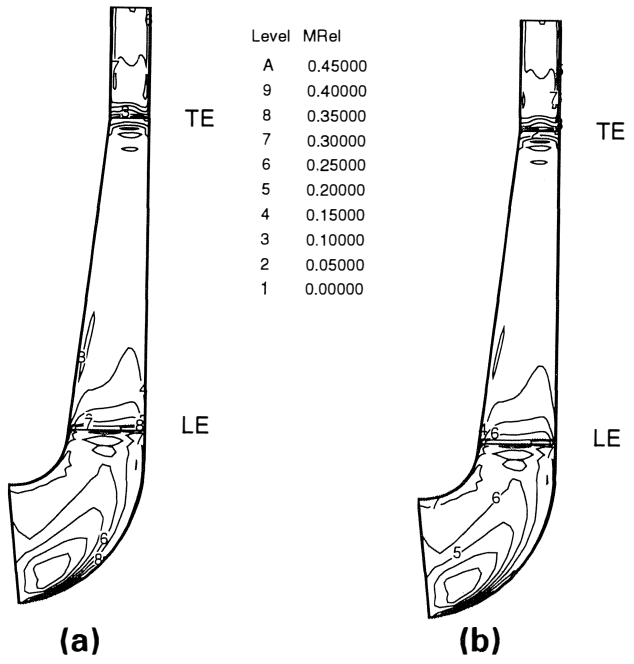

Figure 23. Suction Surface Mach Number Contours. (a) correct blading; (b) blade with lean.

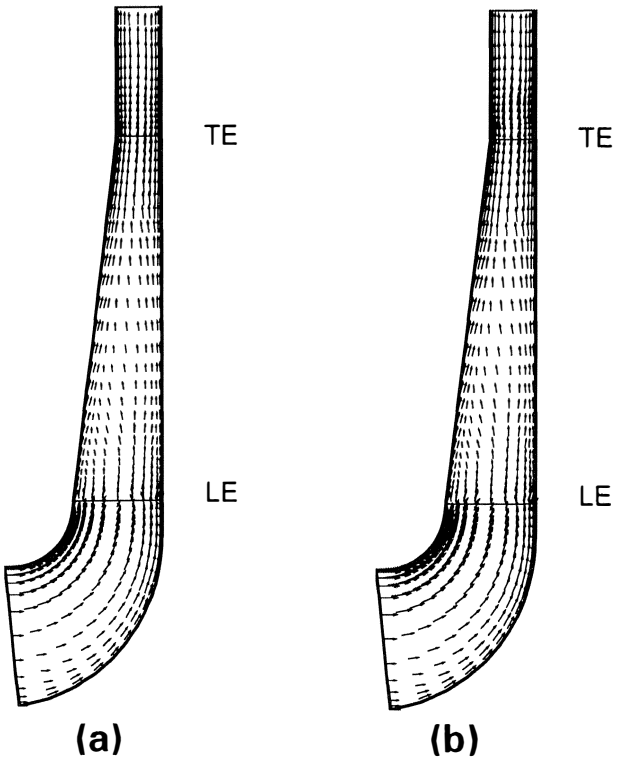

Figure 24. Pressure Surface Velocity Vector Plots. (a) correct blading; (b) blade with lean.

In the first example, CFD results for a poor performing impeller were compared to those from a new design to ensure that problems associated with the old design had been eliminated. In the second example, as-built *vs* design geometries were compared to determine if there were any significant aerodynamic differences. Such comparative studies are valuable since they help the analyst develop 3-D acceptance criteria or guidelines that may be employed to judge future design efforts.

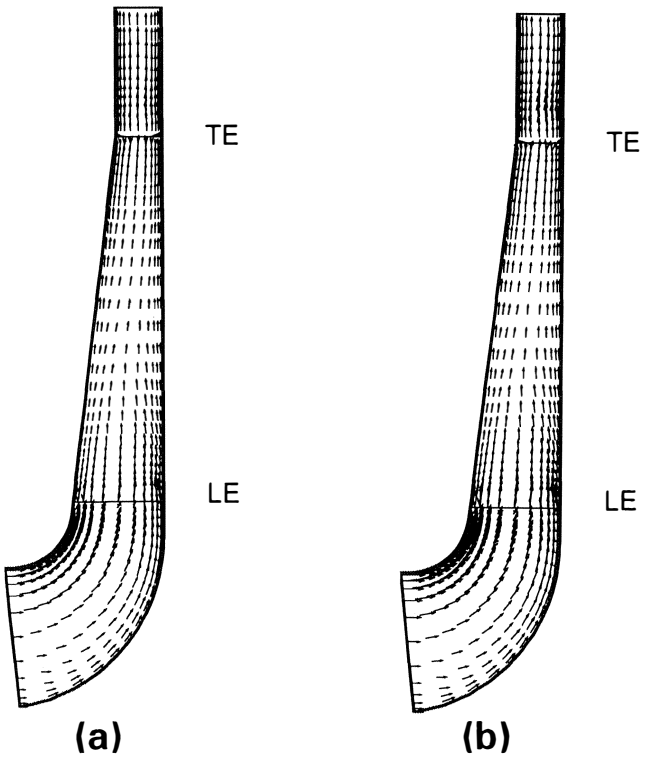

Figure 25. Suction Surface Velocity Vector Plots. (a) correct blading; (b) blade with lean.

FLOW VISUALIZATION

To gain a better understanding of the flow through turbomachinery components, designers often utilize flow visualization. This has typically been done using one of two methods: a) by building a plexiglas (or other transparent material) model of the component; or b) by installing a "window" that allows visual access to the flow passage. Smoke, bubbles, or some other media are passed through the flow channel, allowing visual inspection or laser measurements of the flow profile. Obviously, significant time and money can be expended building a scale model or, if possible, installing a "window" in the actual flow element. Unless frequent use is anticipated, the additional cost of laser anemometry equipment can be prohibitive. Further, such measurements are often ineffective in some operating environments; given the delicate prism/mirror systems required for some systems. Finally, after all of this expense, if the component design is found to be inadequate, a new model or part must be fabricated and the entire test program repeated.

Computational fluid dynamics codes offer a very attractive alternative. Rather than building a component, the flow visualization is computer modelled. The grid becomes the part and the CFD code acts as the flow. In short, the flowfield can be visualized without the use of smoke or mirrors. Of greater importance, if a design is found to be ineffective, the computer model is modified or deleted with no loss of metal, Plexiglas or the like.

The sample results presented are for a high flow coefficient impeller (0.150) that has been used in numerous production compressors and has always performed very well. No details of the impeller design will be addressed. Rather, the discussion will

concentrate on the use of the CFD code to visualize the flow as it passes through the impeller.

Examples of velocity vector plots have been offered earlier herein. While these are very valuable in flowfield visualization, a more effective format is the streakline or particle trace plots. As mentioned earlier, these plots trace the path that a "zero mass" particle (sometimes called pseudo-particles) would follow should it pass through the flow passage. Notably, the plots offered in this paper were actually developed by the PLOT3D postprocessor. That is, the particle trace is performed by the postprocessor rather than the CFD code itself. Some CFD packages will calculate the movement of particulate matter in a flow stream; however, BTOB3D does not have that capability. Therefore, the PLOT3D particle trace was applied.

The observer may note that some of the particles traces seemed to end prematurely. One of the drawbacks of the PLOT3D streakline is that the trace will end if a particle hits a passage surface. For example, if a trace indicates that a particle will strike the blade surface, the trace will end at that point.

To "test" the sample impeller, two operating conditions were run; one at design or peak efficiency flow and one at reduced flow (near surge). For each case, two streakline plots are presented. Pseudo-particle traces along the suction, pressure, and hub surfaces are shown in the first view. In the second plot, the streaklines along the same surfaces as viewed looking directly into the impeller exit are offered. Note, the shroud traces were omitted primarily to ease viewing. Also, at the low flow condition, the shroud traces were truncated as the pseudo-particles made contact with the shroud surface just downstream of the leading edge.

The streaklines at the design flow condition (Figures 26 and 27) show few patterns of interest. The particles tend to move smoothly from inlet to exit with little deviation from the expected flow profile. The only conspicuous trend appears as a spiral that forms along the suction surface, reflecting the wake region that forms in every centrifugal impeller. In general, the flow through this impeller appears to be very well behaved; as might be expected, since prior test data indicating superior performance were available.

Streaklines at the low flow condition are far more interesting (Figures 28 and 29). Here, there appear to be regions of separation along the suction surface (visible as the streaklines form large spirals and/or reverse direction). Of course, this separation is caused by increased leading edge incidence and other factors which are a natural result of the reduction in inlet flow. That is, one should *expect* these patterns at this flow condition. However, the ability to review the patterns resulting from increased incidence levels, etc. offers the designer valuable insight into the impeller's reaction to off-design conditions.

HOLDING CFD IN THE PROPER PERSPECTIVE

There are limitations to computational fluid dynamics codes that must be recognized. While offering the designer an enhanced understanding of the flowfield, the CFD code remains but an approximation of the actual flow characteristics. The greatest uncertainty lies in the modelling of the turbulent flow, and there is disagreement amongst CFD experts as to which model offers the most promise. Numerous models are applied, but each is known to be less than perfect. Therefore, the magnitude of the velocities, pressures, temperatures, etc., calculated by the CFD code can have significant error, especially in the near wall or boundary layer regions of the passage. Consequently, many feel that CFD codes must be treated as a qualitative rather than quantitative tool. That is, the general trends (i.e., velocity profiles) developed by the CFD code will be correct but the absolute values of the results (i.e., velocity levels) may be in error. As turbulence models improve and as codes are calibrated against available test data, the quantitative accuracy will improve.

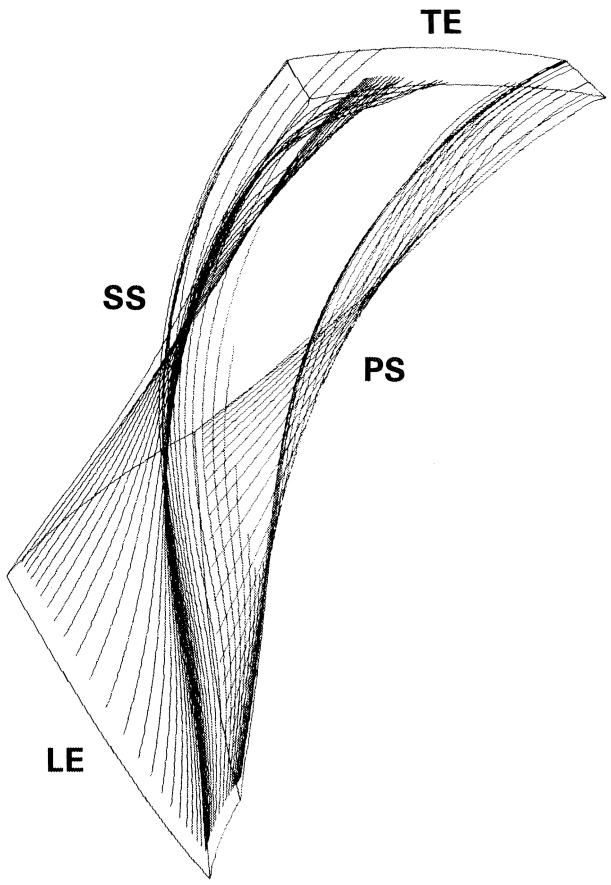

Figure 26. Streaklines Along Pressure, Suction, and Hub Surfaces (Design Flow Condition).

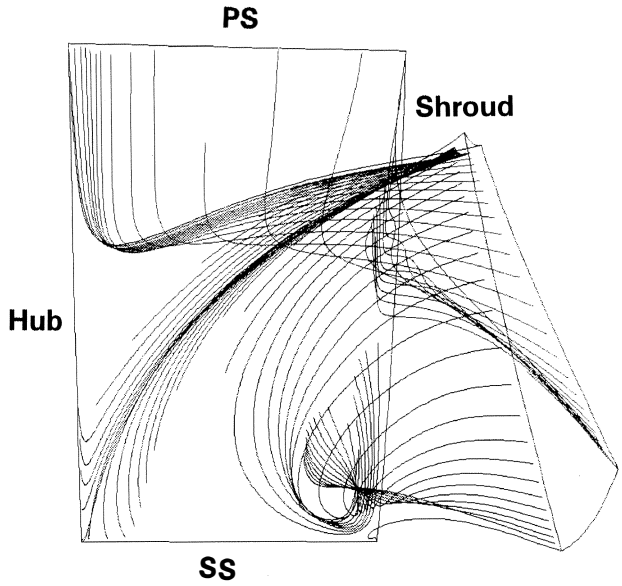

Figure 27. Streaklines Along Pressure, Suction, and Hub Surfaces as Viewed From The Impeller Exit (Design Flow Condition).

It is also important to recognize that 3-D CFD is still a relatively new field. Consequently, the new user must develop an understanding of what constitutes a good *vs* bad result. For example,

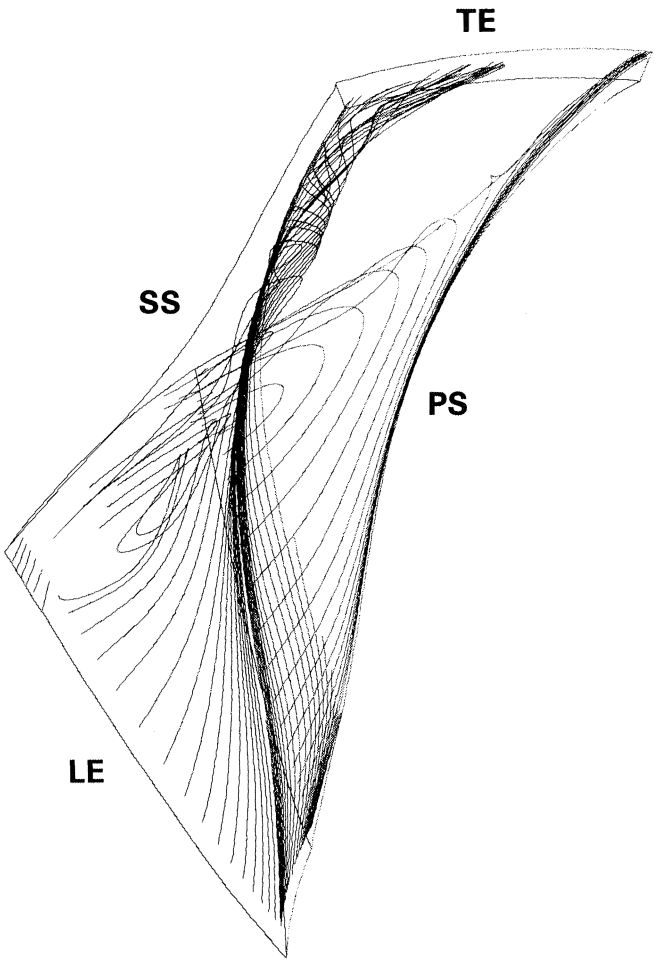

Figure 28. Streaklines Along Pressure, Suction, and Hub Surfaces (Reduced Flow Condition).

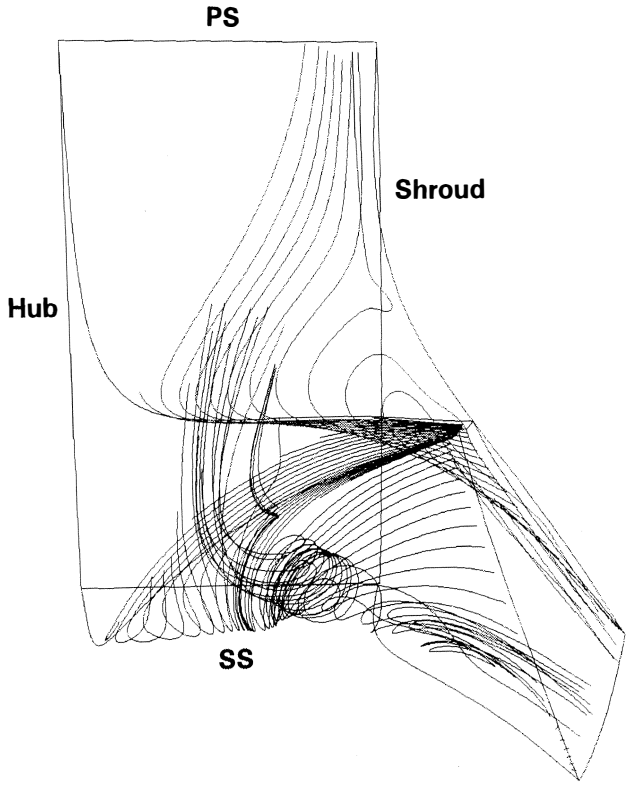

Figure 29. Streaklines Along Pressure, Suction, and Hub Surfaces As Viewed from the Impeller Exit (Reduced Flow Condition).

what constitutes a good velocity vector profile? Do all low mach number or wake regions necessarily reflect an adverse condition? Is it possible to attain high efficiency and good range if CFD results show recirculation zones? What trends are acceptable in off-design CFD results? In short, the new user must gain experience using CFD to develop the necessary judgment criteria for the results obtained from the code.

Finally, the designer must, over time, accumulate test data to validate the results of the CFD code, as it is applied to the various component design styles. The validation process might involve detailed laser measurements of the velocities through a component; or it may be as uncomplicated as comparing mass-averaged CFD results with overall component measured performance. For example, in the latter, test results may show that the CFD code overestimates or underestimates performance for a particular design style. If so, the aerodynamic engineer must to be cognizant of this deviation when completing future designs.

CONCLUSIONS

Computational fluid dynamics may be used in the design of industrial turbomachinery. With the development of the specialized solvers, such as the Dawes code BTOB3D, input preparation efforts and computer run times have been reduced significantly. Therefore, day to day use of the software has become practical.

A brief description of the BTOB3D code was presented and a discussion of the various types of plots used by CFD analysts were offered. This was followed by a discussion of three sample cases, illustrating the effective use of the CFD code as: a) a comparative tool; and b) a flow visualization tool. Finally, comments regarding maintaining the proper perspective on CFD results were presented.

In conclusion, computational fluid dynamics codes have given the designer a very powerful tool in the design/analysis of advanced turbomachinery components. Though they will never replace component testing, the insight such codes offer contribute to a further understanding of turbomachinery flow physics. The results will be higher performance, greater operating range, and, in general, a more effective, efficient turbomachine for the end user.

NOMENCLATURE

A_o	Gas sonic velocity
I	Grid planes in the blade to blade direction
J	Grid planes in the inlet to exit (streamwise) direction
K	Grid planes in the hub to shroud direction
LE	Leading edge
PS	Pressure surface
SS	Suction surface
TE	Trailing edge
U_2	Impeller tip rotational speed = (N D_2)/ 720
ϕ	Flow coefficient = 700 Q/ND_2^3 where: Q = flow in ACFM; N = operating speed in RPM; and D_2 = impeller diameter is inches

BIBLIOGRAPHY

Casey, M.V., Dalbert, P. and Roth, P., "The Use of 3D Viscous Flow Calculations in the Design and Analysis of Industrial Centrifugal Compressors," ASME paper 90-GT-2 (1990).

Dawes, W. N., "Development of a 3D Navier Stokes Solver for Application to all Types of Turbomachinery", ASME paper 88-GT-70 (1988).

Howard, J. H. G. and Osborne, C., "A Centrifugal Compressor Flow Analysis Employing a Jet-Wake Passage Flow Model," ASME paper 76-FE-21 (1976).

Johnson, M. W. and Moore, J., "The Development of Wake Flow in a Centrifugal Impeller," Journal of Engineering for Power, *102*, pp 382-390 (April 1980).

Kitson, S. T., et al., "The Computational Experiment Applied to Aerodynamic Design and Analysis of Turbomachinery," SAE900360, Conference, Detroit, Michigan (1990).

Krain, H. and Hoffman, W., "Verification of an Impeller Design by Laser Measurements and 3D-Viscous Flow Calculations," ASME paper 89-GT-159 (1989).

Sorokes, J.M. and Welch, J.P., "Centrifugal Compressor Performance Enhancement Through The Use Of A Single Stage Development Rig," Proceedings of the Twentieth Turbomachinery Symposium, The Turbomachinery Laboratory, The Texas A&M University System, College Station, pp 101-112 (1991).

ACKNOWLEDGMENTS

The author wishes to acknowledge several individuals whose efforts contributed to the completion of this paper: Edward Bennett of Concepts, ETI, who assisted the author in the implementation of the Dawes code at Dresser-Rand and provided guidance in the interpretation of the results; Jerry Wood of NASA Lewis who provided utility software that eased the postprocessing effort; Jay Koch, David Kirk, Ed Thierman, and Jim Shufelt who assisted the author in generating the various figures. The author also wants to thank Dresser-Rand for allowing publication.